Cysteine Deleted Protegrin-1 (CDP-1): Anti-bacterial Activity, Outer-Membrane Disruption and Selectivity

Harini Mohanram and Surajit Bhattacharjya*

School of Biological Sciences, Structural Biology and Biochemistry, Nanyang Technological University, Singapore 637551.

*Address correspondence to: Surajit Bhattacharjya, School of Biological Sciences, 60 Nanyang Drive, Singapore, 637551, e-mail: surajit@ntu.edu.sg, Fax: 65-6791-3856

Background: Protegin-1 (PG-1: RGGRLCYCRRRFCVCVGR-amide) assumes a rigid β-hairpin like structure that is stabilized by two disulfide bridges between Cys6-Cys15 and Cys8-Cys13. Previous studies, employing linear analogs of PG-1, with Cys to Ala mutations or modified Cys, have demonstrated that the disulfide bridges are critical for the broad spectrum and salt resistant antimicrobial activity of PG-1.

Methods: In order to understand structural and functional roles of disulfide bonds in protegrins, we have synthesized a Cys deleted variant of PG-1 or CDP-1, RGGRLYRRRFVVGR-amide, and two of its analogs, RR11, RLYRRRFVVGR-amide, and LR10, LYRRRFVVGR-amide, containing deletion of residues at the N-terminus. These peptides have been characterized for bactericidal activity and mode of action in lipopolysaccharide (LPS) using optical spectroscopy, ITC and NMR.

Results: Antibacterial activity, against Gram-negative and Gram-positive strains, of the three peptides follows the order: CDP-1>RR11>LR10. LR10 displays only limited activity toward Gram-negative strains. CDP-1 demonstrates efficient membrane permeabilization and high-affinity interactions with LPS. CDP-1 and RR11 both assume β-hairpin like compact structures in complex with LPS, whereas LR10 adopts an extended conformation in LPS. In zwitterionic DPC micelles CDP-1 and the truncated analog peptides do not adopt folded conformations.

Major Conclusions: Despite the absence of stabilizing disulfide bridges CDP-1 shows broad-spectrum antibacterial activity and assumes β-hairpin like structure in complex with LPS. The β-hairpin structure may be essential for outer membrane permeabilization and cell killing.

Keywords: Antimicrobial peptides, Protegrin-1, Lipopolysaccharide, NMR, Antibiotics

1. Introduction

Cationic antimicrobial peptides (AMPs) are an integral part of the host defense mechanisms with broad spectrum activity against bacteria, viruses, fungi, parasites and also to the drug resistant bacteria [1-3]. Due to the bactericidal activity of AMPs toward multiple drug resistant bacteria, AMPs are considered to be promising leads for the new generation of antibiotics [4-7]. The broad spectrum activity of AMPs stems from their ability to destabilize membrane structures of pathogens [8-11]. As a mode of action against Gram-negative bacteria, cationic AMPs would interact with the anionic LPS and permeabilize the outer membrane before gaining access to the inner membrane or to the intra-cellular targets [12-14]. Further, LPS is found to actively regulating insertion, inactivation and synergistic mode of action of antimicrobial peptides including temporins and K/L helical AMPs [15-17]. LPS, also termed endotoxin, is involved in a number of human diseases including septic shock syndromes for which currently there is no therapeutics modality [18-20]. AMPs could be a promising source for the development of LPS neutralizing drugs [21-25]. Atomic-resolution structures of AMPs in complex with LPS, therefore, are vital to correlate mechanism of action of host defense AMPs [26-31].

Protegrins are highly potent broad spectrum cationic β-hairpin AMPs derived from leucocytes of porcine [32]. Among five members, protegrin-1 (PG-1) has drawn considerable attention for antimicrobial drug development [32-37]. Iseganan or IB367 an analog of PG-1 has been evaluated in a phase three clinical trial for oral mucositis [34]. A rigid β-hairpin structure containing two antiparallel β-sheets of protegrin-1 (PG-1) is stabilized by two internal disulfide bridges between Cys6-Cys15 and Cys8-Cys13 (Table 1) [38, 39]. As a

mode of action, PG-1 appears to be permeabilizing bacterial membranes including the outer membrane of Gram-negative bacteria [31, 36]. Structural studies have demonstrated that the β-hairpin conformation of PG-1, although monomeric in free solution [38,39], may form oligomeric β-sheet like structures in zwitterionic detergent micelles and model lipid bilayers [40,41]. It has been proposed that these oligomeric β-sheet states of PG-1 can induce pore formation in bacterial membrane causing cell lysis [40-43].

Structural and functional implications of the disulfide bridges of PG-1 are found to be of interest [44-48]. Mutations of the four Cys residues with Ala or the chemical modification of the free thiols of reduced Cys residues have yielded largely inactive analogs of PG-1 [44, 45]. Further, removal of one of the disulfide bridges, between Cys6-Cys15, has resulted in a more loss of bactericidal activity in comparison to the analog containing a disulfide bridge between Cys8-Cys13 [44]. Stabilization of the β-hairpin conformation, using D-Pro at the turn and replacing Cys residues with β-sheet promoting residues, was found to be necessary to generate active linear analogs of PG-1 [47, 48]. These aforementioned studies have replaced Cys with other residues or thiol groups of four Cys were chemically modified. These changes might affect conformations and membrane interactions of the linear analogs. Removal of Cys residues could be an attractive approach for the development of simple shorter linear analogs of disulfide containing AMPs [49, 50]. Here, we have synthesized Cys deleted protegrin-1 (CDP-1) and two of its N-terminal truncated variants, RR11 and LR10. In order to understand mode of action of the linear analogs of PG-1 in outer membrane, we have carried out LPS interactions of these three peptides, using optical and biophysical methods, in terms of outer membrane disruption, LPS binding affinity, and perturbation of LPS structures. Further, CD and NMR spectroscopy, in complex with LPS and DPC micelles, have been utilized to gain

structural insights for LPS recognition and lipid selective interactions of CDP-1, RR11 and LR10 peptides.

2. Materials and methods

2.1 Peptide synthesis, purification and lipids

All peptides, CDP-1, RR11 and LR10, were commercially synthesized by GL Biochem, (Shanghai, China). Peptides were purified through a linear gradient of 90% water and 10% acetonitrile with 0.1% TFA in reverse phase HPLC (Waters), using a C_{18} column (300 Å pore size, 5 μm particle size). The portion of the peak eluting with high absorbance was collected and lyophilized for further experiments. The molecular weight of the peptides, CDP-1 (1747.10 da), RR11 (1476.81 da) and LR10 (1320.62 da) were confirmed with mass spectroscopy. All peptides were >98% pure. LPS of *E. coli* 0111:B4 (purified through ion-exchange chromatography), fluorescein isothiocyanate (FITC) labelled LPS (2-10 μg of FITC per mg of LPS) of *E. coli* 055:B5 were purchased from Sigma-Aldrich, St. Louis, MO. Per deuterated DPC-d_{38} and DPC were obtained from Cambridge Isotope Laboratories Inc. and Avanti Polar Lipids, respectively. All other chemicals were of analytical grades.

2.2 Bacteria

E. coli of Gram-negative bacteria and *B. subtilis* of Gram-positive bacteria are lab strains. Other strains like *P. aeruginosa* ATCC 27853, *K. pneumoniae* ATCC 13883 and *S. enterica* ATCC 14028 of Gram-negative bacteria and *S. aureus* ATCC 25923, *S. pyogenes* ATCC 19615 and *E. faecalis* ATCC 29212 of Gram-postive bacteria were obtained from American type culture collection, (Rockville, MD).

2.3 Determination of minimum inhibitory concentration (MIC)

Mid-log phase of bacterial strains were obtained in MH (Mueller-Hinton) broth from overnight culture and diluted to OD_{600} of 0.01 (~$3.8X10^6$ CFU/ml). About 25 μL of two-fold serial dilution of peptides in water were made in 96-well polypropylene plates with equal volume of diluted bacterial strains. Polypropylene plates were then incubated at 37°C for 16 hours. Bacterial growth were measured spectrophotometrically at 600 nm and wells showing least OD values at 600 nm were streaked onto MH agar plates and incubated at 37°C overnight. Plates with no visible bacterial colonies correspond to MIC value of peptides.

2.4 Membrane permeability of intact E. coli cells

Fluorescence emission spectra of 1-N-Phenylnaphthyl-amine (NPN), (Sigma-Aldrich, St. Louis, MO) and SYTOX green (Invitrogen) were obtained at various concentrations of CDP-1, RR11 and LR10 peptides in *E. coli* cell solutions. Actively growing mid-log phase of *E. coli* cells were obtained in LB (Luria-Bertanii) broth and diluted to OD_{600} of 0.5 ($1.9X10^8$ CFU/ml) in 10 mM sodium phosphate buffer, pH 6.8. Membrane permeabilization assays were performed in phosphate buffer solutions, rather than in MH broth medium, due to lower light scattering effect in buffer solutions. Basal fluorescence spectra of the probe molecules, either with 10 μM NPN or 1 μM of SYTOX green, were obtained with excitation at 350 nm and 485 nm, respectively. Increasing concentrations of peptides were added to the cells following recording of emission spectra of NPN and SYTOX green. Further, NPN uptake assays were also performed in 10 mM Tris buffer, pH 7.2 containing 20 mM $CaCl_2$ determining effect of divalent counter ions in the outer membrane permeabilization. About 50 μM of polymyxin B (PMB) (Sigma-Aldrich) was added to achieve the complete lysis of the cells. The fluorescence intensity change was calculated by

% of fluorescent increase =[($I_{peptide}$-I_{blank})/(I_{PMB}-I_{blank})] *100, where $I_{peptide}$, I_{blank} and I_{PMB} are fluorescent intensities after addition of peptides, before addition of peptides and after addition of PMB, respectively.

2.5 Isothermal titration calorimetry (ITC) experiments

Thermodynamic parameters of binding interactions of peptides with LPS micelles were determined using ITC (VP-ITC, Microcal Inc, Northampton, MA). Samples of peptides, LPS and DPC micelles were prepared in 10 mM sodium phosphate buffer, pH 6.8 and filtered. Ideally, 25 injections of 3.5 μL of 1 mM peptide were sequentially made into 0.01 mM of LPS, in the sample cell at 25^{o}C and 37 ^{o}C. The molecular weight of LPS has been considered as 10 KD [51]. During experiments, the sample cell was spin continuously at 300 rpm and peptide solution was injected at an interval of 3 mins. Peptide-DPC micelle interactions were carried out in Microcal ITC_{200}. About 25 injections of 0.5 μL of 1 mM peptides were continuously made into 5 mM DPC micelles in sample cells at 25 ^{o}C. Raw ITC data were analysed using one site binding model by Microcal Origin 5.0 software provided with the instrument. Association constant (K_a) and enthalpy change (ΔH) could be directly estimated from ITC data. ΔG and $T\Delta S$ were calculated from the fundamental equations of thermodynamics, $\Delta G = -RT\ln K_a$ and $T\Delta S=(\Delta H-\Delta G)$, respectively.

2.6 Interactions of FITC labelled LPS with peptides

Fluorescence emission spectra of FITC conjugated LPS were obtained at various concentrations of peptides probing changes of self-association of LPS. Fluorescence emission of 500 nM of FITC-LPS was recorded in the absence and presence of increasing concentrations of the peptides in 10 mM sodium phosphate buffer, pH 7.0. The excitation was set at 480 nm and emission spectra were collected at 500-550 nm. A 10 μL of 10% (v/v)

aqueous Triton X-100 was added finally to record the complete dissociation of LPS micelles. The change of fluorescence intensity was estimated as, % of fluorescent increase =[($I_{peptide}$-I_{blank})/($I_{tritonX100}$-I_{blank})] *100, where $I_{peptide}$, I_{blank} and $I_{tritonX100}$ are fluorescent intensities after addition of peptides, before addition of peptides and after addition of tritonX100, respectively.

2.7 Circular dichroism (CD) spectroscopy of peptides in LPS and DPC micelles

Global conformational changes of CDP-1, RR11 and LR10 peptides were measured using far UV-CD spectroscopy in LPS and DPC micelles. CD data were collected using a Chirascan CD spectrometer (Applied Photophysics Ltd., UK). Peptides in free solutions and peptide/micelle complexes were scanned from 190 to 240 nm wavelengths in a 0.01 cm. path length of cuvette for an average of 3 scans. Baseline scans were acquired using 10 mM sodium phosphate buffer, pH 7.0. LPS and DPC micelles baselines were also acquired with same settings. For CD studies concentration of each peptide was fixed at 50 μM whereas 30 μM of LPS and 20 mM DPC were added for complexes. CD data of samples were subtracted from baselines and corrected data were converted to molar ellipticity.

2.8 NMR spectroscopy of peptides and structure calculations

NMR experiments were conducted on a Bruker DRX 600 spectrometer, equipped with the cryo-probe and pulse field gradients. Data acquisition and processing were performed with the Topspin software (Bruker) running on a Linux workstation. Two dimensional TOCSY (total correlation spectroscopy) and NOESY (nuclear overhauser effect spectroscopy) spectra of all three peptides, 0.5 mM concentration, in free solution were acquired in aqueous solution containing 10 % D_2O at pH 4.5 at 25^oC. NMR spectra were acquired at lower pH value of 4.5 to obtain sharper amide proton signals. The mixing times for TOCSY and NOESY for free peptides were set to 80 ms and 250 ms respectively. DSS (2,2-dimethyl-2-

silapentane 5-sulfonate sodium salt) was used as an internal standard for chemical shift. For interactions of peptide-LPS, 1-D NMR spectra of individual peptide were acquired at different concentrations of LPS ranging from 5 μM to 50 μM. Note, that the critical micelle concentrations of LPS of *E. coli* 0111:B4 has been determined to be ~ 1 μM and the micelle sizes of LPS remained unchanged till 50 μM of LPS [51, 52]. 2-D transferred NOESY (tr-NOESY) experiments were carried out with a mixture of peptide, 0.5 mM and LPS 50 μM, at three different mixing time, 100, 150 and 200 ms. NOE intensities at these mixing times were utilized to generate NOE build up curve. For NMR experiments of peptides in DPC micelles, 0.5 mM peptide was dissolved in 125 mM DPC-d_{38}. Two dimensional TOCSY and NOESY spectra were obtained at 308 K. NMR spectra of DPC-bound peptides were found to be better resolved at higher temperature, 35^{o}C, in comparison to 25^{o}C, presumably due to the faster tumbling of the micelle-peptide complexes [9]. NMR derived structures of CDP-1 and analogs were calculated using CYANA program [53]. Sequence-specific resonance assignments of each peptide were achieved by standard procedure [54]. Intensity of NOEs were categorized to strong, medium and weak and translated to upper bound distance limits to 2.5, 3.5 and 5.0 Å, respectively. Out of 100 structures calculated, 20 lowest energy structures were kept for analyses. PROCHECK was used to analyse Ramachandran plot for the validation of structures calculated. A model of the complex of CDP-1 and LPS was generated from an iterative docking using INSIGHTII program. The atomic coordinates of LPS were derived from cocrystal structure of LPS and Fhu A (1QFG). During docking, backbone conformation of CDP-1 and conformation of LPS were kept fixed, while sidechain dihedral angles of basic amino acids of CDP-1 were varied to maximizing ionic interactions among the phosphate groups of LPS/lipid A. The LPS-peptide model was further energy minimized using steepest descent algorithm.

3. Results

3.1 Antibacterial activity of CDP-1, RR11 and LR10 peptides

We have determined the minimal inhibitory concentration (MIC) of CDP-1, RR11 and LR10 peptides against four Gram-negative and four Gram-positive bacterial strains in MH broth medium (Table 2). CDP-1 displays bactericidal activity against Gram-negative and Gram-positive strains with low MIC values ranging between 2 μM to 8 μM. By contrast, deletion analogs, RR11 and LR10 peptides demonstrate higher MIC values in comparison to CDP-1. As, RR11 peptide is moderately bactericidal with MICs of 8 μM to 25 μM, whereas LR10 peptide contains significantly higher MICs >200 μM for Gram-negative strains (Table 2). These results demonstrate that the N-terminus sequence R^1GGR^4 motif of CDP-1 is important for the abroad spectrum antibacterial activity. In particular, a large difference in MIC values for Gram-negative bacteria between RR11 and LR10 peptides indicates critical role of residue R4 in bacterial selectivity. It may be noted that an N-terminal deletion analog, of the RGGR sequence motif, of PG-1 has also exhibited a significant loss of bactericidal activity [37].

3.2 Membrane disruption of E. coli by CDP-1, RR11 and LR10 peptides

Peptide induced membrane perturbation of *E. coli* cells has been investigated using fluorescence emission of hydrophobic dyes, 1-N-phenylnapthylamine (NPN) and SYTOX green. These fluorescent probes are excluded from cells due to the permeability barrier of cell membranes and showed fluorescence emission spectra of low intensity. Structural perturbation of the outer membrane facilitates uptake of NPN into the non-polar environment of membrane components, which results an enhancement of the intensity of fluorescence. On the other hand, the fluorescence intensity of SYTOX green increases in complex with nucleic

acids of cells. The linear analogs, CDP-1, RR11 and LR10, of PG-1 delineate permeabilization of *E. coli* cell membranes with different efficacies. Fig. 1A shows percentage of fluorescence increase by linear analogs of PG-1 normalized to PMB. There have been dramatic increases in membrane permeabilizing ability with increasing concentrations of CDP-1 (Fig. 1A). By contrast, changes in fluorescence intensity of NPN with response to RR11 and LR10 peptides are relatively lower in comparison to CDP-1, whereby LR10 shows the least fluorescence changes among the three peptides. All peptides including CDP-1 demonstrate significantly lower outer membrane permeabilization, as judged by the limited increase of NPN fluorescence, in the presence of 20 mM $CaCl_2$ (Fig. S1). These observations indicate that electrostatic interactions between peptides and outer membrane are critical for membrane permeabilization. Note, electrostatic interactions have been known to be playing dominant roles in binding of cationic AMPs with the outer and inner membrane of bacteria [1,2].

In SYTOX green assays CDP-1 induces an efficient efflux of the dye into cytoplasm of *E. coli* cells. Fig. 1B shows percentage of fluorescence increase by linear analogs of PG-1 normalized to PMB. SYTOX green in *E. coli* cell solutions have experienced a considerable increase in fluorescence emission intensity upon inclusion of CDP-1 in a dose dependent manner (Fig. 1B). By contrast, fluorescence intensity increase of SYTOX green has been limited in the presence of truncated peptides RR11 and LR10 (Fig. 1B). Taken together, NPN and SYTOX green uptake results clearly indicate that CDP-1 is highly efficient in disrupting the outer membrane barrier and also permeabilize inner membrane integrity of *E. coli* cells. On the other hand, RR11 and LR10 peptides demonstrate moderate and low outer-membrane permeabilization, respectively.

3.3 Binding affinity of CDP-1, RR11 and LR10 to LPS micelles

LPS-peptides interactions are quantified using isothermal titration calorimetry (ITC) experiments. ITC experiments were carried out at 25 ^{o}C and 37 ^{o}C in 10 mM sodium phosphate buffer (see Materials and Methods). In ITC studies, aliquots of CDP-1, RR11 and LR10 peptides were added, in individual experiments, to a fixed concentration of LPS solution until heat changes were saturated (Fig. 2, panels A-C, Fig. S2). Binding three peptides with LPS micelles appear to be exothermic in nature at both temperatures as indicated by the downward position of ITC peaks (Fig. 2, panels A-C, Fig. S2); revealing enthalpy driven binding interactions. ITC data are fitted into the one site binding model to determine thermodynamic parameters and interactions affinity (Table 3). ITC analyses delineate that LPS binding affinity of three peptides follows the order: CDP-1>RR11>LR10. Since, the apparent dissociation constant (K_d) values are estimated to be 0.35 μM, 0.96 μM and 3 μM for CDP-1, RR11, LR10, respectively (Table 3). ITC experiments were also carried out for CDP-1, RR11 and LR10 peptides with zwitterionic DPC micelles. Peptides-DPC micelles interactions appeared to be highly low-affinity as indicated by the lack of saturation and lower heat changes in ITC (Fig. S3).

3.4 Dissociation of LPS micelles by CDP-1, RR11 and LR10 peptides

LPS forms aggregated structures of micelles in solution [51, 52]. Binding of LPS binding proteins and potent AMPs to such aggregated structures may induce perturbation and dissociation of LPS micelles as previously demonstrated [15, 55, 56]. Fluorescence emission intensity of FITC is quenched in LPS aggregated micelles due to energy transfer among the chromophores [55, 56]. Disaggregation of LPS micelles would increase fluorescence emission intensity of FITC following the release of self-quenching effect [55, 56]. FITC fluorescence emission spectra of FITC-LPS were acquired in the absence of peptides, in 10% Triton-X solution for complete disaggregation of LPS micelles and in the presence of various

concentrations of CDP-1, RR11 and LR10 peptides (Fig. S4). As can be seen, FITC-LPS fluorescence intensity is highly limited in the absence of Triton-X and protegrin linear peptides (Fig. S4). Fig. 3 shows percentage fluorescence emission intensity increase at 515 nm wavelength of FITC-LPS in the presence three peptides at their increasing concentrations. As can be seen, the fluorescence intensity of FITC increases with the additions of CDP-1, RR11 and LR10 peptides (Fig. 3). CDP-1 induces a much larger increase of FITC fluorescence intensity in comparison to RR11 and LR10 peptides (Fig. 3). These data demonstrate that LPS micelles are more significantly perturbed or dissociated upon binding to CDP-1 peptide.

3.5 Secondary structures of CDP-1, RR11 and LR10 peptides

Far UV CD spectroscopy was used to obtain conformations of the three peptides, at 50 μM, in free aqueous solution and in solutions containing 30 μM LPS and 20 mM DPC (Fig. 4). CD spectra of CDP-1 (Fig. 4A), RR11 (Fig. 4B) and LR10 (Fig. 4C) in aqueous solutions and also in DPC detergent micelles demarcate one intense minima of negative ellipticity at θ_M ~ 195-200 nm which is characteristics of disordered or random conformations of polypeptides. By contrast, in LPS containing solutions CD spectra of CDP-1 (Fig. 4A), RR11 (Fig. 4B) and LR10 (Fig. 4C) are defined by two dominant CD bands at 210 nm and 195-198 nm of negative and positive ellipticity, respectively. Such CD spectral features represent rather non-random conformations of these peptides in LPS micelles. In particular, CD band observed at 210 nm for CDP-1, RR11 and LR10 peptides may indicate populations of β-type or β-turn like conformations [57]. Some CD signals can be seen ~ 230-240 nm that may account for a contribution from aromatic amino acids of these peptides [57]. Taken together, CD studies have demonstrated that LPS binding stabilizes non-random structures, plausibly β-types, to

CDP-1 and also for its two analogs, RR11 and LR10. However, all three peptides assume largely random conformations in the context of zwitterionic DPC micelles and also in free solutions.

3.6 NMR spectroscopy of CDP-1, RR11 and LR10

Conformational characteristics of CDP-1, RR11 and LR10 peptides have been examined by two-dimensional (2-D) ^{1}H-^{1}H NMR in free solution, in DPC micelles and in LPS micelles. Sequence-specific resonance assignments for all three peptides were achieved by analyses of 2-D TOCSY and NOESY spectra [54]. 2-D NOESY spectra of CDP-1, RR11 and LR10 peptides in water and in solutions containing DPC micelles showed limited number of NOEs (Figs. S5-S8). Most of these NOEs are either of intra-residue and sequential in nature (Fig. S8). Also, the secondary chemical shifts of αH resonances of the three peptides have experienced a limited deviation from random coil values (Fig. S8). These observations indicated that a lack of populated folded conformations of CDP-1, RR11 and LR10 peptides under these solution conditions.

Atomic solution structures of AMPs in complex with LPS can be determined using transferred nuclear Overhauser effect spectroscopy (tr-NOESY), whereby AMPs-LPS interactions are in fast exchange in NMR time scale [27-30]. In tr-NOESY, LPS bound NOEs are detected in the chemical shifts of the free peptide in solution [27-30]. A series of 1-D NMR spectra were recorded for CDP-1, RR11 and LR10 peptides at various concentrations of LPS (see Materials and Methods). Additions of LPS had caused broadening of NMR spectra of the peptides, indicating LPS-peptides interactions are in fast exchange regime (Fig. S9). tr-NOESY spectra of CDP-1, RR11 and LR10 display NOE contacts involving proton resonances of backbone/backbone, backbone/sidechain and sidechain/sidechain (Fig 5). In

addition, NOE build-up curves showed a linear relationship with mixing times, suggesting absence of spin diffusion effect (Fig. S10). Analyses of tr-NOESY spectra of CDP-1 and RR11 have revealed sequential, medium range and a number of long-range NOEs (Fig. 5 and Fig. 6). In particular, long-range NOEs for CDP-1 can be seen among residues R4/V12, R4/V11, R4/G13, G3/R14 (Table 4). In addition, there are NOEs among aromatic ring protons of residueY6 and residue F10. RR11 peptide delineates fewer long-range NOEs involving residues Y6/V12 and Y6/R14 (Fig 6B). By contrast, NOE connectivities of LR10 peptide in LPS micelles are found to be sequential and medium range without any long-range NOE contacts (Fig. 6C).

3.7 LPS-bound 3-D structures of CDP-1, RR11 and LR10 peptides

LPS-bound structures of CDP-1, RR11 and LR10 peptides were determined based on tr-NOE driven distance constrains of 104, 102 and 88, respectively, using CYANA (Table 5). Fig. 7 shows superposition of backbone atoms (C^{α}, N, and C') of an ensemble of structures of CDP-1 (panel A), RR11 (panel B) and LR10 (panel C). The RMSD values for backbone (C^{α}, N, and C') atoms and all heavy atoms from the mean structure were estimated to be; CDP-1: 0.4 Å and 1.0 Å, RR11: 0.03 Å and 0.9 Å, LR10: 0.27 Å, 1.19 Å respectively (Table 5). In complex with LPS, CDP-1 and RR11 assume β-hairpin like structures, whereas LR10 adopts extended or β-strand like conformation (Fig. 8). The central residues Y6-R7-R8-R9 of CDP-1 adopt a β-turn conformation causing the chain reversal of β-hairpin structure (Fig. 8A). In the β-turn, the carbonyl oxygen atom of residue L7 is in close proximity, 2.7 Å, to the amide nitrogen atom of residue R9, indicating a potential hydrogen bond. The guanidinium sidechains of residues R7 and R8 located at i+1 and i+2 positions, respectively, of the β-turn are extended out of the plane of β-hairpin structure. In the β-hairpin structure of CDP-1, N-

terminal residues G3-R4-L5 and C-terminal residues F10-V11-V12 are found be forming the part of the two antiparallel β-strands (Fig. 8B). Further, the two β-strands of the β-hairpin of CDP-1 are characterized by potential hydrogen bonds between the carbonyl oxygen atom of residue G3 and the nitrogen atom of residue V11, (C=O---N~ 4 Å), and the carbonyl oxygen atom of residue R9 and the nitrogen atom of residue L5, (C=O---N~ 2.7 Å), (Fig. 8B). The guanidinium sidechains of residues R4, R14, R7, R8 and R9 are oriented along one face of the β-hairpin, whereas sidechains of aromatic and hydrophobic residues Y6, F10, V11 and V12 occupy the opposite side giving rise to an amphipathic structure (Fig. 8B). The β-hairpin structure of RR11 demonstrates a different packing and sidechain topology unlike the β-hairpin of CDP-1. The β-turn structure of RR11 is sustained by residues R7-R8-R9-F10 of which residues R8 and R9 are occupying i+1 and i+2 positions in the turn (Fig 8C). In addition, the carbonyl oxygen atom of residue R7 is in proximity, 3.7 Å, to the amide nitrogen of residue F10, suggesting a potential hydrogen bond in the β-turn. In the β-hairpin structure of RR11, the sidechains of residues Y6, R8, R9, F10, V12 and R4 constitute one face of the β-hairpin, whereas sidechains of residues L5, R7, V11 and R14 are placed along the other side the β-hairpin (Fig. 8D). In other words, the β-hairpin structure of RR11 peptide is less amphipathic in comparison to that of CDP-1. By contrast, the LPS-bound structure of LR10 peptide has been defined by an extended strand containing multiple local turn-like structures (Fig. 8E). In particular, residues R8-R9-F10-V11 may form a β-turn with a potential hydrogen bond between the carbonyl oxygen atom of R8, (C=O---N~ 2.7 Å), with the amide hydrogen of V11 (Fig. 8E). A three residue γ-turn can also be found including residues V11-V12-G13 which may be defined by a yet another hydrogen bonding involving the carbonyl oxygen atom of residue V11 (C=O---N~ 3.6 Å), and the amide hydrogen residue G13 (Fig. 8E).

4. Discussion

4.1 Antibacterial activity, bacterial membrane permeabilization and LPS Binding by CDP-1 and analogs

AMPs are promising leads for the next generation antibiotics for the eradication of drug resistance pathogens [3, 4, 6]. Understanding of structure activity correlations of AMPs can potentially generate improved and effective antimicrobials and designed novel mimetics [8-11]. Amphipathic characteristics of AMPs are considered to be vital for the membrane perturbation and cell lysis [1, 2, 13]. Consequently, inter-relationship of cationicity and hydrophobicity in amphipathic AMPs has been addressed in several occasions [8.9]. Many SAR studies have been carried out using liposomes or bilayers of synthetic lipids that may potentially mimic the inner membrane of bacteria [8, 9,11]. The LPS-outer membrane is an important component for the mode of action of AMPs toward Gram-negative pathogens [13, 16, 21, 22]. 3-D structures and interactions of AMPs in LPS lipid are of considerable interest to develop broad-spectrum antibiotics and anti-endotoxin materials [13, 21, 26-29]. Toward this, atomic resolution structures of a number of potent helical AMPs including MSI-594, pardaxin, temporin L, have been recently reported [26-29]. By contrast, atomic resolution structures and interactions of β-sheets or β-hairpin AMPs in LPS have not been well studied [31,44,50]. Due to the high importance of protegrins in antimicrobial drug development, here, we have investigated disulfide deleted variants, CDP-1, RR11 and LR10 of PG-1. The antibacterial activity of CDP-1 and N-terminal deleted variants, RR11 and LR10, correlated well with their ability to disrupt membrane integrity and binding to LPS-outer membrane. In bactericidal assays, CDP-1 has been found to be highly potent against Gram-negative and Gram-positive bacteria. PG-1 delineated somewhat reduced MICs, ranging from 0.5 to 2 μM against different bacterial cells [44, 45]. The truncated analogs of CDP-1, RR11 and LR10

peptides, demonstrated higher MIC values. In particular, LR10 has been found to be rather inactive against Gram-negative bacteria (Table 2). We find that CDP-1 has demonstrated a higher efficacy in outer membrane and inner membrane disruption compared to RR11 and LR10 peptides (Fig. 1). At MIC concentration of 4 μM for CDP-1, the extent of NPN uptake was estimated to be ~ 20% (Fig 1A). However, it may be noted that the membrane permeabilization measurements were carried out at 50 times higher cell density in compared to MIC assays. At 30 μM CDP-1 concentration, a dye uptake of ~90% was observed (Fig 1A). A similar trend of perturbation was also detected in SYTOX green assays. At 4 μM of CDP-1 concentration, 28% of dye uptake has occurred that further increases to 97% at 30 μM concentration (Fig 1B). RR11 and LR10 peptides could reveal approximately 70% and 40% of NPN uptake at 30 μM concentrations, respectively (Fig 1A). However, in SYTOX green assays, both RR11 and LR10 peptides delineated similar inner membrane permeabilization (Fig. 1B). Thus, these cells based membrane permeabilization data strongly correlate with the bactericidal activity of CDP-1, RR11 and LR10 peptides. In particular, the broad spectrum antibacterial activity of CDP-1 results from its ability to disrupt the LPS outer membrane and inner plasma membrane of bacteria. Whereas, reduced activity of LR10 peptide against Gram-negative bacteria (MIC > 200 μM) might be occurring due to the low permeabilization of LPS-outer membrane. Moreover, disruption of LPS micelle structures and LPS binding affinity, evaluated from FITC-LPS fluorescence and ITC studies, respectively, of CDP-1, RR11 and LR10 peptides support their spectrum of antibacterial activity. CDP-1 interacted with LPS micelles with low micro molar affinity and binding of the CDP-1 to LPS micelles have rendered disruption of higher-order micellar structures of LPS. These observations might indicate that CDP-1 may potentially disrupt the structural organization of the outer membrane leading to plausible permeabilization of the cell wall. Vis-a-vis, both the truncated

peptides, RR11 and LR10, show limited LPS binding affinity and structural changes of LPS micelles causing their reduced antibacterial and outer membrane permeabilization activity. Peptides-LPS interactions appear to be dictated by electrostatic interactions as suggested by reduced LPS-outer membrane permeabilization by CDP-1 in the presence of counter ions Ca^{2+} (Fig. S1) and the exothermic heats observed in ITC experiments (Fig. 2, Fig. S2). Notably, AMPs-LPS interactions investigated by ITC are often found to be endothermic, below the phase transition temperature of LPS, at 25^{o}C [58-61]. Such endothermic or entropy driven binding between LPS-AMPs has been interpreted as release of water molecules from phosphate groups of LPS upon complex formation [62,63]. However, observation of an exothermic binding, at 25 ^{o}C, between LPS and CDP-1 including two of its analogs may be noteworthy. We speculated that electrostatic interactions between cationic residues of CDP-1 peptides with negatively charged LPS might be predominating over the entropy gain caused by the release of water molecules. As many as six Arg residues, similar to PG-1, in the primary structure of CDP-1 may be involved in LPS interactions and consequent disruption of the outer membrane barrier. Since, deletion analogs, RR11 and LR10 lacking one or two Arg residues, respectively, have demonstrated significantly diminution in LPS binding affinity and outer membrane permeabilization. In other words, the N-terminal sequence motif RGGR of CDP-1 appears to be critical in contributing LPS binding and outer membrane permeabilization.

4.2 Conformations and selectively of CDP-1, RR11 and LR10 peptides

CD and NMR spectral characteristics delineated that all three peptides are largely unstructured in free aqueous solutions. Solution NMR has shown that PG-1 is folded in a β-hairpin structure with two disulfide bridges in free solution [38, 39]. Conformations of PG-1 have also been examined in solution containing zwitterionic DPC micelles by NMR. This

study has found that β-hairpin structure of PG-1 has interacted with DPC micelles and further assembled into anti-parallel dimers [41]. It has been concluded that several of these dimers may form oligomers in lipid or detergent environments. Solid-state NMR studies carried out in model lipid bilayers composed of either of zwitterionic or negatively charged lipids have demonstrated that β-hairpin of PG-1 forms β-sheet oligomers or β-barrel like structures on these membrane surfaces, respectively [40]. Interestingly, none of these linear analogs, CDP-1, RR11 and LR10 of PG-1 show interactions and conformational transitions in zwitterionic DPC micelles. CD and NMR studies revealed absence of well-defined structures for CDP-1, RR11 and LR10 peptides in solutions containing DPC micelles (Fig. 4 and Fig. S8). By contrast, CDP-1, RR11 and LR10 peptides interact and assume structures in complex with negatively charged LPS micelles. In other words, the disulfide deleted linear analog of PG-1 or CDP-1 is bestowed with interactions with the negatively charged lipids like LPS. It may be noted that PG-1, plausibly due to its interactions with zwitterionic lipids, contains hemolytic activity against human RBC [64]. Atomic-resolution structures of CDP-1, RR11 and LR10 obtained in complex with LPS provide important mechanistic insights toward the antimicrobial and membrane permeabilization activities. As seen, CDP1- and RR11 peptides assume β-hairpin like structures whilst a rather β-strand like conformation has been determined for LR10 peptide in complex with LPS. A weak LPS outer-membrane permeabilization and high MIC values for Gram-negative bacteria of LR10 peptide may be directly related to its inability to fold into the β-hairpin like structure in LPS lipids. Thus, the β-hairpin like conformations of linear peptides CDP-1, RR11 including the native PG-1, are highly essential for antibacterial activity. Although, RR11 peptide assumes the β-hairpin like backbone fold, however, the β-hairpin structure of RR11 lacks an amphipathic disposition in terms of the orientation of the sidechains of residues (Fig. 8D). Consequently, a lower

potency in antimicrobial and cell membrane permeabilization activities of RR11 peptide, compared to CDP-1, may be arising from non-amphipathic structure in LPS. As shown in a number of studies that the structural amphipathicity of AMPs are vital for their broad spectrum activity [1-3]. On the other hand, the β-hairpin structure of CDP-1 demonstrates an amphipathic disposition of sidechains of residues (Fig. 8B). To obtain a structural model of LPS-CDP-1 interactions, the β-hairpin structure of CDP-1 was iteratively docked with the lipid A domain of LPS (Fig. 9). The LPS/CDP-1 complex may be sustained by a number of salt-bridges and/or hydrogen bonds among the anionic phosphate groups of the lipid A moiety and positively charged sidechains of Arg residues. For instance, the guanidinium sidechains of residues R1, R4 and R14 are in close proximity to the di-phosphate groups at the O1 position of glucosamine I. Whereas, the guanidinium sidechains of residues R7 and R8 are in close contact with the O4 monophosphate group of glucosamine II. In addition, the sidechains of non-polar and aromatic residues including L5, Y6, F10, V11 and V12 make intimate van der Waals packing contacts with the fatty acyl chains of LPS (Fig. 9). These mutual non-covalent interactions may potentially be stabilizing LPS/CDP-1 complex and causing a disruption of integrity of LPS layer at the outer membrane. Further, the docked structure of LPS/CDP-1 shows an involvement of the N-terminal cationic residues R1 and R4 in ionic interactions with the phosphate groups of the lipid A moiety of LPS. These interactions will be potentially absent in case of N-terminal deleted peptides including LR10 that would underscore significantly reduced LPS binding affinity and also acquisition of β-hairpin like structure of LR10 in complex with LPS.

5. Conclusion

AMPs and derived analogs provide a novel source of anti-infective agents with different mode of action that may be essential to combat drug-resistant bacteria. Structure-activity

correlations of existing or naturally occurring AMPs can generate new scaffolds for discovery of broad spectrum antibiotics. In this work, we have demonstrated that CDP-1, the Cys deleted analog of PG-1, exert a broad spectrum antibacterial activity and interacted with the negatively charged lipid like LPS. As a mode of action, CDP-1 disrupts LPS-outer membrane permeability barrier and possibly traverse to the inner plasma membrane. CDP-1 assumes an amphipathic β-hairpin like conformation, even in the absence of disulfide bonds, in complex with LPS micelles. The β-hairpin structure may insert into LPS lipid plausibly cause disorganize of packing of LPS outer membrane. The N-terminal sequence motif RGGR of CDP-1 has been observed to be important for activity and formation of the β-hairpin structure in LPS. We surmise that CDP-1 may be utilized for the development of simple non-toxic antimicrobials with enhanced binding affinity for endotoxin.

Acknowledgements: This work was supported by a grant RG11/12 from the Ministry of Education, Singapore.

References

1. M Zasloff, Antimicrobial peptides of multicellular organisms, Nature 415 (2002) 389-395.
2. K.A. Brogden, Antimicrobial peptides: pore formers or metabolic inhibitors in bacteria? Nat Rev Microbiol 3 (2005) 238-250.
3. E. Guani-Guerra, T. Santos-Mendoza, S.O. Lugo-Reyes, L.M. Teran, Antimicrobial peptides: general overview and clinical implications in human health and disease, Clin Immunol 135 (2010) 1-11.
4. P.C. Oyston, M.A. Fox, S.J. Richards, G.C. Clark, Novel peptide therapeutics for treatment of infections, J Med Microbiol 58 (2009) 977-987.
5. C. Avitabile, F. Netti, G. Orefice, M. Palmieri, N. Nocerino, G. Malgieri, L.D. D'Andrea, R. Capparelli, R. Fattorusso, A. Romanelli, Design, structural and functional characterization

of a Temporin-1b analog active against Gram-negative bacteria, Biochim Biophys Acta 1830 (2013) 3767-3775.

6. J.L. Fox. Antimicrobial peptides stage a comeback, Nature Biotechnology 31 (2013) 379-382.

7. G. Wang, Database guided discovery of potent peptides to combat HIV-1 or superbugs, Pharmaceuticals 6 (2013) 728-758.

8. C.D. Fjell, J.A. Hiss, R.E. Hancock, G. Schneider, Designing antimicrobial peptides: form follows function, Nat Rev Drug Discov 11 (2012) 37-51.

9. L.T. Nguyen, E.F. Haney, H.J. Vogel, The expanding scope of antimicrobial peptide structures and their modes of action, Trends Biotechnol 29 (2011) 464-472.

10. Y Shai, Mode of action of membrane active antimicrobial peptides, Biopolymers 66 (2002) 236-248.

11. W.C. Wimley, Describing the mechanism of antimicrobial peptide action with the interfacial activity model, ACS Chem Biol 5 (2010) 905-917.

12. D.S. Snyder, T.J. McIntosh, The lipopolysaccharide barrier: correlation of antibiotic susceptibility with antibiotic permeability and fluorescent probe binding kinetics. Biochemistry 39 (2000) 11777-11787.

13. S. Bhattacharjya, A. Ramamoorthy, Multifunctional host defense peptides: functional and mechanistic insights from NMR structures of potent antimicrobial peptides, FEBS J 276 (2009) 6465-6473.

14. L. Ding, L. Yang, T. M. Weiss, A. J. Waring, R. I. Lehrer, H.W. Huang, Interaction of antimicrobial peptides with lipopolysaccharides, Biochemistry 42 (2003) 12251-12259.

15. N. Papo, Y. Shai, A molecular mechanism for lipopolysaccharide protection of gram-negative bacteria from antimicrobial peptides, J Biol Chem 280 (2005) 10378-10387.

16. Y. Rosenfeld, D. Barra, M. Simmaco, Y. Shai, M.L. Mangoni, A synergism between temporins toward gram-negative bacteria overcomes resistance imposed by the lipopolysaccharide protective layer, J Biol Chem 281 (2006) 28565-28574.

17. R. Saravanan, M. Joshi, H. Mohanram, A. Bhunia, M. L. Mangoni, S. Bhattacharjya, NMR structure of temporin-1 Ta in lipopolysaccharide micelles: mechanistic insight into inactivation by outer membrane, PLoS ONE 8 (2013) e72718.

18. C.R. Raetz, C. Whitfield, Lipopolysaccharide endotoxin. Annu Rev Biochem 71 (2002) 635-700.

19. J. Cohen, The immunopathogenesis of sepsis, Nature 420 (2002) 885-891.
20. G.S. Martin, D.M. Mannino, S. Eaton, M. Moss, The epidemiology of sepsis in the United States from 1979 through 2000, N Engl J Med 348 (2003) 1546-1554.
21. S. Bhattacharjya, De novo designed lipopolysaccharide binding peptides: structure based development of antiendotoxic and antimicrobial drugs, Curr Med Chem 17 (2010) 3080-3093.
22. N.Y. Yount, M.R. Yeaman, Peptide antimicrobials: cell wall as a bacterial target, Ann N Y Acad Sci 1277 (2013) 127-138.
23. M.G. Scott, A.C. Vreugdenhil, W.A. Buurman, R.E. Hancock, M. R. Gold, Cutting edge: cationic antimicrobial peptides block the binding of lipopolysaccharide (LPS) to LPS binding protein, J Immunol 164 (2000) 549-553.
24. T. Schuerholz, S. Domming, M. Hornef, A. Dupont, I. Kowalski, Y. Kaconis, L. Heinbockel, J. Andra, P. Garidel, T.Gutsmann, S. David, S. Sanchez-Gomez, G. M. Tejada, K. Brandenburg, Bacterial cell wall compounds as promising targets of antimicrobial agents II. Immunological and clinical aspects. Curr Drug Targets 13 (2012) 1121-1130.
25. R. Dings, J. R. Haseman, D.B. Leslie, M. Luong, D. L. Dunn, K. H. Mayo, Bacterial membrane disrupting dodecapeptide SC4 improves survival of mice challenged with *Pseudomonas aeruginosa*, Biochim Biophys Acta 1830 (2013) 3454-3457.
26. A. Bhunia, R. Saravanan, H. Mohanram, M. L. Mangoni, S. Bhattacharjya, NMR structures and interactions of temporin-1Tl and temporin-1Tb with lipopolysaccharide micelles: mechanistic insights into outer membrane permeabilization and synergistic activity, J. Biol Chem 286 (2011);286:24394-24406.
27. B. Japelj, P. Pristovsek, A. Majerle, R. Jerala, Structural origin of endotoxin neutralization and antimicrobial activity of a lactoferrin-based peptide, J Biol Chem 280 (2005)16955-16961.
28. A. Bhunia, A. Ramamoorthy, S. Bhattacharjya, Helical hairpin structure of a potent antimicrobial peptide MSI-594 in lipopolysaccharide micelles by NMR spectroscopy. Chemistry 15 (2009) 2036-2040.
29. P.N. Domadia, A. Bhunia, A. Ramamoorthy, S. Bhattacharjya, Structure, interactions, and antibacterial activities of MSI-594 derived mutant peptide MSI-594F5A in lipopolysaccharide micelles: role of the helical hairpin conformation in outer-membrane permeabilization. J Am Chem Soc 132 (2010);132:18417-18428.

30. S. Bhattacharjya, P. Domadia, A. Bhunia, S. Malladi, S. David, High resolution solution structure of a designed peptide bound to lipopolysaccharide: transferred nuclear Overhauser effects, micelle selectivity and anti-endotoxic activity, Biochemistry 46 (2007) 5864-5874.
31. T. Kushibiki, M. Kamiya, T. Aizawa, Y. Kumaki, T. Kikukawa, M. Mizuguchi, M. Demura, S. Kawabata, K. Kawano, Interaction between tachyplesin I, an antimicrobial peptide derived from horseshoe crab, and lipopolysaccharide, Biochim Biophys Acta. 1844 (2014) 527-534.
32. V.N. Kokryakov, S.S.L. Harwig, E.A. Panyutich, A.A. Shevchenko, G.M. Aleshina, O.V. Shamova, H.A. Korneva, R.I. Lehrer, Protegrins-leukocyte antimicrobial peptides that combine features of corticostatic defensins and tachyplesins, FEBS Lett 327 (1993) 231-236.
33. J. Chen, T.J. Falla, H. Liu, M.A. Hurst, C.A. Fujii, D.A. Mosca, J.R. Embree, D.J. Loury, P.A. Radel, C. Chang, L. Gu, J.C. Fiddes, Development of protegrins for the treatment and prevention of oral mucositis: structure-activity relationships of synthetic protegrin analogues, Biopolymers 55 (2000) 88-88.
34. H. Tamamura, T. Murakami, S. Horiuchi, K. Sugihara, A. Otaka, W. Takada, T. Ibuka, M. Waki, N. Yamamoto, N. Fujii, Synthesis of protegrin-related peptides and their antibacterial and anti-human immunodeficiency virus activity, Chem Pharm Bull 43 (1995) 853-858.
35. D. Gidalevitz, Y. Ishitsuka, A.S. Muresan, O. Konovalov, A.J. Waring, R.I. Lehrer, K.Y. Lee, Interaction of antimicrobial peptide protegrin with biomembranes, Proc Natl Acad Sci U S A. 100 (2003) 6302-6307.
36. N. Ostberg, Y. Kaznessis, Protegrin structure–activity relationships: using homology models of synthetic sequences to determine structural characteristics important for activity, Peptides 26 (2005) 197-206.
37. L. M. Gottler, R. Salud Bea, C.E. Shelburne, A. Ramamoorthy, E.N. Marsh, Using fluorous amino acids to probe the effects of changing hydrophobicity on the physical and biological properties of the beta-hairpin antimicrobial peptide protegrin-1, Biochemistry 47 (2008) 9243-9250
38. R. L. Fahrner, T. Dieckmann, S.S.L. Harwig, R.I. Lehrer, D. Eisenberg, J. Feigon, Solution structure of protegrin-1, a broad-spectrum antimicrobial peptide from porcine leukocytes, Chem Biol 3 (1996) 543-550.

39. A. Aumelas, M. Mangoni, C. Roumestand, L. Chiche, E. Despaux, G. Grassy, B. Calas, A. Chavanieu, Synthesis and solution structure of the antimicrobial peptide protegrin-1. Eur J Biochem 237 (1996) 575-583.

40. R. Mani, S.D. Cady, M. Tang, A.J. Waring, R.I. Lehrer, M. Hong, Membrane-dependent oligomeric structure and pore formation of a beta-hairpin antimicrobial peptide in lipid bilayers from solid-state NMR, Proc Natl Acad Sci U S A. 103 (2006) 16242-16247.

41. C. Roumestand, V. Louis, A. Aumelas, G. Grassy, B. Calas, A. Chavanieu, Oligomerization of protegrin-1 in the presence of DPC micelles. A proton high-resolution NMR study, FEBS Lett 421 (1999) 263-267.

42. A.A. Langham, A.S. Ahmad, Y.N. Kaznessis, On the nature of antimicrobial activity: a model for protegrin-1 pores, J Am Chem Soc 130 (2008) 338-346.

43. T. Lazaridis, Y. He, L. Prieto, Membrane interactions and pore formation by the antimicrobial peptide protegrin, Biophys J 104 (2013) 633-642.

44. S.S. Harwig, A. Waring, H.J. Yang, Y. Cho, L. Tan, R.I. Lehrer, Intramolecular disulfide bonds enhance the antimicrobial and lytic activities of protegrins at physiological sodium chloride concentrations Eur J Biochem 240 (1996) 352-357.

45. M.E. Mangoni, A. Aumelas, P. Charnet, C. Roumestand, L. Chiche, E. Despaux, G. Grassy, B. Calas, A. Chavanieu, Change in membrane permeability induced by protegrin 1: implication of disulphide bridges for pore formation, FEBS Lett 383 (1996) 93-98.

46. J.P. Tam, C. Wu, J.L. Yang, Membranolytic selectivity of cystine-stabilized cyclic protegrins Eur J Biochem 267 (2000) 3289-3300.

47. J.R. Lai, B.R. Huck, B. Weisblum, S.H. Gellman, Design of non-cysteine-containing antimicrobial beta-hairpins: structure-activity relationship studies with linear protegrin-1 analogues. Biochemistry 41 (2002) 12835-12842.

48. J.R. Lai, R.F. Epand, B. Weisblum, R.M. Epand, S.H. Gellman, Roles of salt and conformation in the biological and physicochemical behavior of protegrin-1 and designed analogues: correlation of antimicrobial, hemolytic, and lipid bilayer-perturbing activities, Biochemistry 45 (2006) 15718-15730.

49. A. Ramamoorthy, S. Thennarasu, A. Tan, K. Gottipati, S. Sreekumar, D.L. Heyl, F.Y. An, C.E. Shelburne, Deletion of all cysteines in tachyplesin I abolishes hemolytic activity and retains antimicrobial activity and lipopolysaccharide selective binding, Biochemistry 45 (2006) 6529-6540.

50. R. Saravanan, H. Mohanram, M. Joshi, P.N. Domadia, J. Torres, C. Ruedl, S. Bhattacharjya, Structure, activity and interactions of the cysteine deleted analog of tachyplesin-1 with lipopolysaccharide micelle: Mechanistic insights into outer-membrane permeabilization and endotoxin neutralization, Biochim Biophys Acta 1818 (2012) 1613-1624.

51. C. A. Aurell, A. O. Wistrom, Critical aggregation concentrations of gram-negative bacterial lipopolysaccharides (LPS), Biochem. Biophys. Res. Commun. 253 (1998) 119-123.

52. L. Yu, M. Tan, B. Hob, J. L. Ding, T. Wohland, Determination of critical micelle concentrations and aggregation numbers by fluorescence correlation spectroscopy: aggregation of a lipopolysaccharide, Analytica Chimica Acta 556 (2006) 216-225.

53. P. Guntert, Automated NMR protein structure calculation with CYANA, Meth Mol Biol 278 (2004) 353-378.

54. K. Wuthrich, NMR of proteins and nueclic acids, New York: John Wiley and Sons, 1986.

55. Y. Rosenfeld, N. Papo, Y. Shai, Endotoxin (lipopolysaccharide) neutralization by innate immunity host-defense peptides: peptide properties and plausible mode of action, J Biol Chem 281, (2006) 1636-1643.

56. P.S. Tobias, K. Soldau, J. A. Gegner, D. Mintz, R. J. Ulevitch, Lipopolysaccharide binding protein-mediated complexation of lipopolysaccharide with soluble CD4, J Biol Chem 270, (1995) 10482-10488.

57. K. Nakanishi, N. Berove, R.W. Woody, Circular dichroism:principles and applications, New York:John Wiley and Sons, 2000.

58. S. Srimal, N. Surolia, S. Balasubramanian, A. Surolia, Titration calorimetric studies to elucidate the specificity of the interactions of polymyxin B with lipopolysaccharides and lipid A, Biochem.J. 315 (1996) 679-686.

59. A. Bhunia, P.N. Domadia, S. Bhattacharjya S, Structural and thermodynamic analyses of the interaction between melittin and lipopolysaccharide, Biochim Biophys Acta 1768 (2007) 3282-3291.

60. A. Bhunia, P. Domadia, J. Torres, K.J. Hallock, A. Ramamoorthy, S. Bhattacharjya, NMR structure of pardaxin, a pore-forming antimicrobial peptide, in lipopolysaccharide micelles: mechanism of outer membrane permeabilization, J Biol Chem 285 (2010) 3883-3895.

61. A. Bhunia, H. Mohanram, P.N. Domadia, J. Torres, S. Bhattacharjya, Designed beta-boomerang antiendotoxic and antimicrobial peptides: structures and activities in lipopolysaccharide, J Biol Chem 284 (2009) 21991-22004.
62. J. Howe, J. Andra, R. Conde, M. Iriarte, P. Garidel, M.H. Koch, T. Gutsmann, I. Moriyon K. Brandenburg, Thermodynamic analysis of the lipopolysaccharide-dependent resistance of gram-negative bacteria against polymyxin B, Biophys J 92 (2007) 2796-2805.
63. K. Brandenburg, A. David, J. Howe, M.H. Koch, J. Andra, P. Garidel, Temperature dependence of the binding of endotoxins to the polycationic peptides polymyxin B and its nonapeptide, Biophys J 88 (2005),1845-1858.
64. L. Bellm, R.I. Lehrer, T. Ganz, Protegrins: new antibiotics of mammalian origin. Exp Opin Invest Drugs 9 (2000)1731-1742.

Figure legends

Figure 1: (A) Plot showing changes in fluorescence intensity, in terms of percentage normalized with respect to PMB, of NPN as a function of concentrations of CDP-1, RR1 and LR10 peptides, demonstrating outer membrane permeabilization. (B) Plot showing changes in fluorescence intensity, in terms of percentage normalized with PMB, of SYTOX green dye as function of concentrations of CDP-1, RR1 and LR10 peptides, demonstrating outer and inner membrane permeabilization. All lines along the data points are for guiding the eyes.

Figure 2: (upper panels A-C) ITC thermograms of LPS binding to CDP-1, RR11 and LR10 peptides. (lower panels A-C) Plots showing molar ratios of LPS:peptides as a function of heat of binding. Data (lower panels A-C) represent best-fitted points according to one site binding mode. ITC experiments were carried out at 25^{o}C, 10 mM sodium phosphate buffer, pH 6.8.

Figure 3: Plot showing changes in fluorescence intensity of FITC of FITC-LPS, in terms of percentage normalized with respect to Triton-X100, as a function of concentrations of CDP-1, RR1 and LR10 peptides. Fluorescence experiments were performed at 10 mM sodium phosphate buffer, pH 7.0. The excitation of FITC was set to 480 nm and emission was collected from 500-550 nm. All lines along the data points are for guiding the eyes

Figure 4: Far UV CD spectra of CDP-1, RR11 and LR10 peptides in free aqueous solutions, solution containing LPS and solution containing DPC micelles. CD spectra were at 10 mM sodium phosphate buffer, pH 7.0.

Figure 5: Selected regions of the two-dimensional ^{1}H-^{1}H tr-NOESY spectra of (A) CDP-1, (B) RR11 and (C) LR10 peptides in the presence of 50 μM LPS at 25^{o}C showing NOE cross-

peaks involving low-field shifted (ω_2-^{1}H) amide protons and aromatic sidechain protons resonances with up-field shifted (ω_1-^{1}H) aliphatic proton resonances.

Figure 6: Bar diagrams summarizing number and types (intra, sequential, medium-range and long-range) of NOEs of CDP-1, RR11 and LR10 peptides in complex with LPS used for structure determination,

Figure 7: Superposition of twenty lowest energy structures of (A) CDP-1, (B) RR11 and (C) LR10 peptides bound to LPS micelles determined using CYANA.

Figure 8: Representative LPS bound structures and sidechain orientation topology of (A-B) CDP-1, (C-D) RR11 and (E) LR10 peptide.

Figure 9: A model of the complex of β-hairpin structure of CDP-1 with LPS showing plausible interactions and mode of binding. The complex may stabilize by ionic and/or hydrogen bond interactions among phosphate groups of the lipid A with sidechains of basic residues of CDP-1. The acyl chains of LPS are in close proximity with the aromatic and nonpolar sidechains of residues of CDP-1. The model was constructed using INSIGHTII molecular modelling software.

Table 1: Amino acid sequences of peptides used in this study.

Peptide	Primary structure
PG-1[a]	R-G-G-R-L-C^{6}-Y-C^{8}-R-R-R-F-C^{13}-V-C^{15}-V-G-R
CDP-1	R-G-G-R-L-Y-R-R-R-F-V-V-G-R
RR11	R-L-Y-R-R-R-F-V-V-G-R
LR10	L-Y-R-R-R-F-V-V-G-R

[a] PG-1 sequence is included for comparison.

Table 2: Minimal inhibitory concentration (MIC, in μM) of CDP-1, RR11 and LR10 peptides

	CDP-1	RR11	LR10
Gram-negative			
E. coli (lab strain)	4	10	50
P. aeruginosa ATCC 27853	8	25	200
K. pneumoniae ATCC 13883	8	25	>200
S. enterica ATCC 14028	8	25	200
Gram-positive			
B. subtilis (lab strain)	8	10	50
S. aureus ATCC 25923	2	8	25
S. pyogenes ATCC 19615	8	25	50
E. faecalis ATCC 29212	4	25	25

Table 3: Thermodynamic parameters derived from binding interactions of CDP-1, RR11 and LR10 peptides with LPS at 25^{o}C.

	CDP-1	RR11	LR10
K_a (μM^{-1})	2.79	1.04	0.33
ΔH ($kcal.mol^{-1)}$	-5.4±2.1	-8.5±4.2	-5.1±1.6
$T\Delta S$ ($kcal.mol^{-1}deg^{-1}$)	3.3	-0.29	2.4
ΔG ($kcal.mol^{-1}$)	-8.7	-8.2	-7.5
K_d (µM)	0.35±0.06	0.96±0.15	3±0.07

Table 4: List of long range NOEs for CDP-1 and RR11 in LPS micelles.

CDP-1		RR11	
Val^{12} HG11	- Arg^{4}HA	Arg^{4} QB	- Val^{8}NH
Val^{12} HG12	- Arg^{4}HA	Arg^{6} QG	- Tyr^{3}QD
Val^{11} HB	- Leu^{5}HA	Arg^{6} QB	- Tyr^{3}QE
Val^{11} HB	- Arg^{4}HA	Arg^{11} HA	- Tyr^{3}NH
Arg^{14} HB	- Gly^{3}NH	Val^{9} HG21	- Tyr^{3}QE
Arg^{14} QG	- Gly^{3}NH	Val^{9} HG11	- Tyr^{3}QE
Arg^{4} QG	- Gly^{13}HA	Val^{9} HG21	- Tyr^{3}NH
Arg^{4} QB	- Gly^{13}HA	Val^{9} HG11	- Tyr^{3}NH
Tyr^{6} HA	- Phe^{10}NH		
Phe^{10} HB	- Tyr^{6}QD		
Phe^{10} HB	- Tyr^{6}QE		
Phe^{10} HA	- Tyr^{6}NH		
Phe^{10} QD	- Tyr^{6}QD		
Phe^{10} QD	- Tyr^{6}QE		

Table 5: Structural statistics summary for twenty lowest energy structures of peptides bound to LPS micelles.

	CDP-1	RR11	LR10
Distance restraints			
intraresidue ($\|i-j\| =0$)	43	41	37
sequential ($\|i-j\| = 1$)	40	37	34
medium range ($2\leq \|i-j\|\leq 4$)	11	20	17
long range ($\|i-j\| \leq 5$)	8	6	0
total NOE constraints	102	104	88
Deviation from mean structure			
backbone atoms (N,Cα, C`) (Å)	0.4	0.03	0.27
heavy atoms (Å)	1.0	0.98	1.19
Ramachandran plot for the mean structure			
% residues in the most favourable and additionally allowed regions	100	100	71.5
% residues in the generously allowed region	0	0	28.5
% residues in the disallowed region.	0	0	0

Figure 1

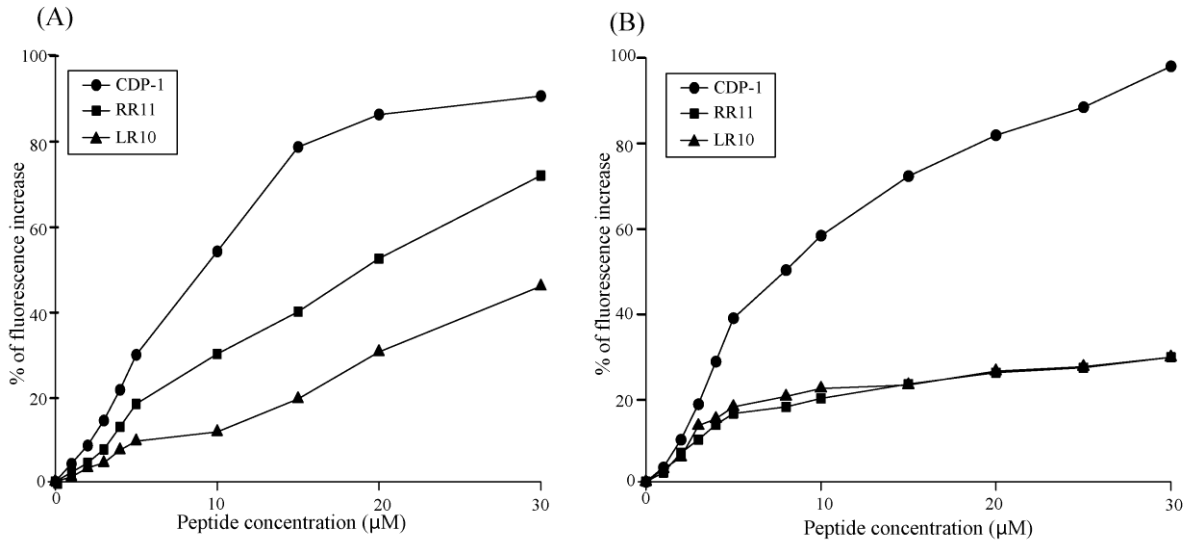
(A)
CDP-1
RR11
LR10
% of fluorescence increase
Peptide concentration (μM)
(B)
CDP-1
RR11
LR10
% of fluorescence increase
Peptide concentration (μM)

Figure 2

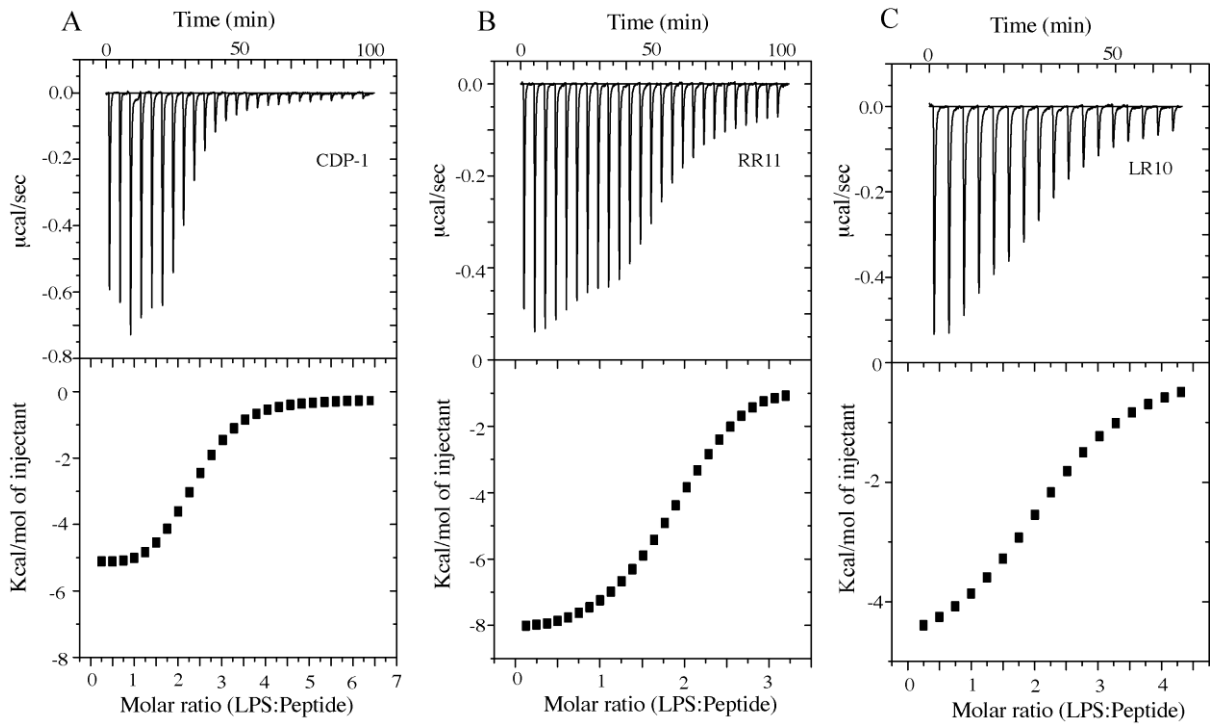
A
Time (min)
0
50
100
0.0
-0.2
-0.4
-0.6
-0.8
µcal/sec
CDP-1
0
-2
-4
-6
-8
Kcal/mol of injectant
0 1 2 3 4 5 6 7
Molar ratio (LPS:Peptide)
B
Time (min)
0
50
100
0.0
-0.2
-0.4
0
µcal/sec
RR11
0
-2
-4
-6
-8
Kcal/mol of injectant
0 1 2 3
Molar ratio (LPS:Peptide)
C
Time (min)
0
50
0.0
-0.2
-0.4
0
µcal/sec
LR10
0
-2
-4
Kcal/mol of injectant
0 1 2 3 4
Molar ratio (LPS:Peptide)

Figure 3

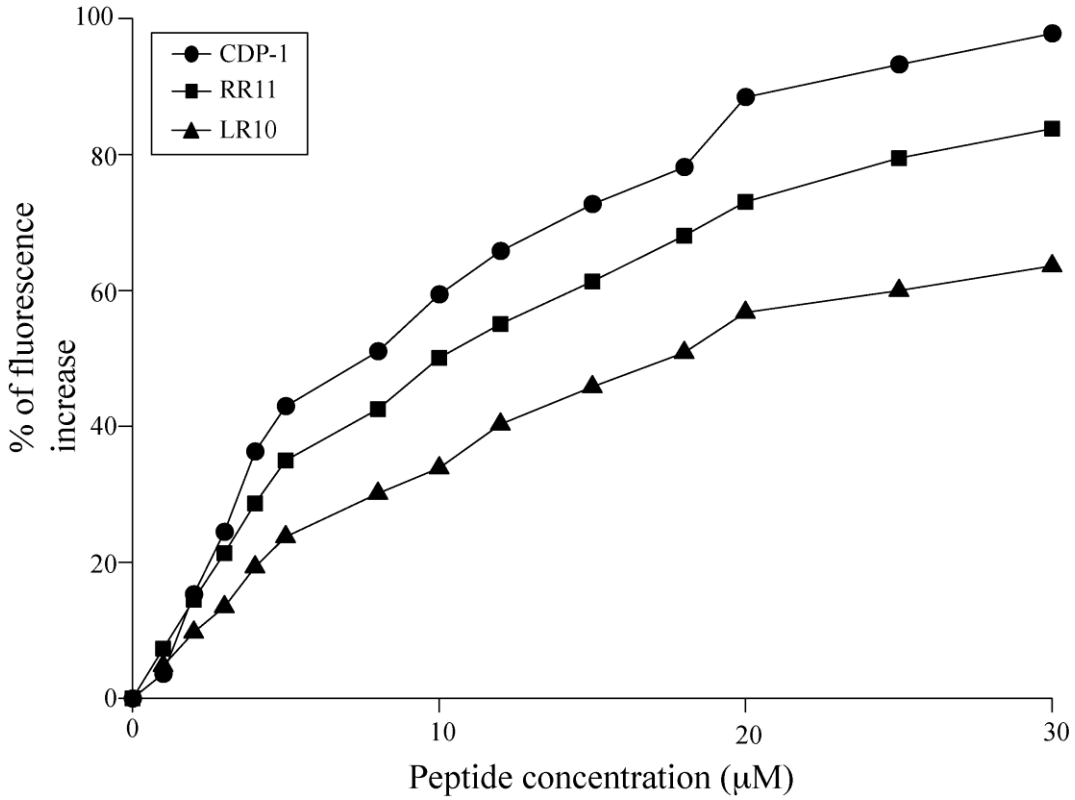
CDP-1
RR11
LR10
% of fluorescence increase
Peptide concentration (μM)
0
20
40
60
80
100
0
10
20
30

Figure 4

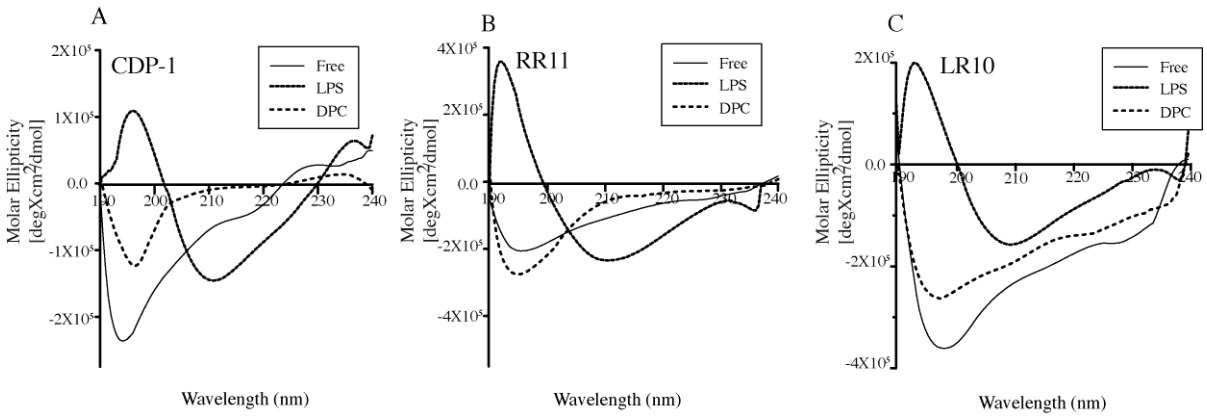
A
CDP-1
Free
LPS
DPC
2X10⁵
1X10⁵
0.0
-1X10⁵
-2X10⁵
Molar Ellipticity [degXcm²/dmol]
190
200
210
220
230
240
Wavelength (nm)
B
RR11
Free
LPS
DPC
4X10⁵
2X10⁵
0.0
-2X10⁵
-4X10⁵
Molar Ellipticity [degXcm²/dmol]
190
200
210
220
230
240
Wavelength (nm)
C
LR10
Free
LPS
DPC
2X10⁵
0.0
-2X10⁵
-4X10⁵
Molar Ellipticity [degXcm²/dmol]
190
200
210
220
230
240
Wavelength (nm)

Figure 5

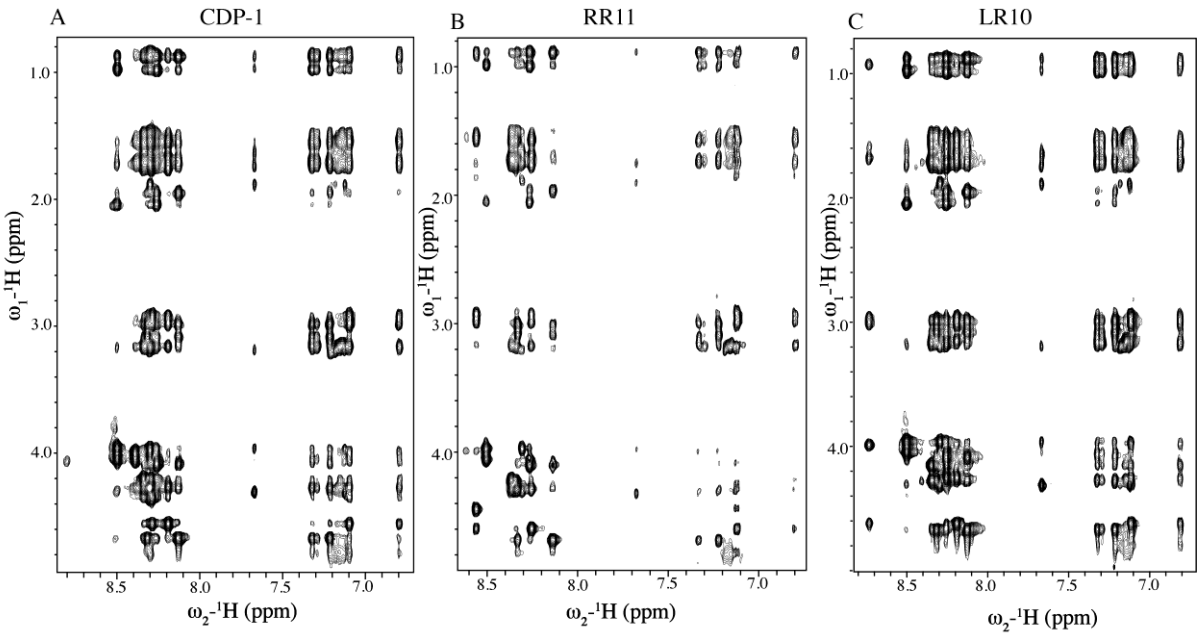

Figure 6

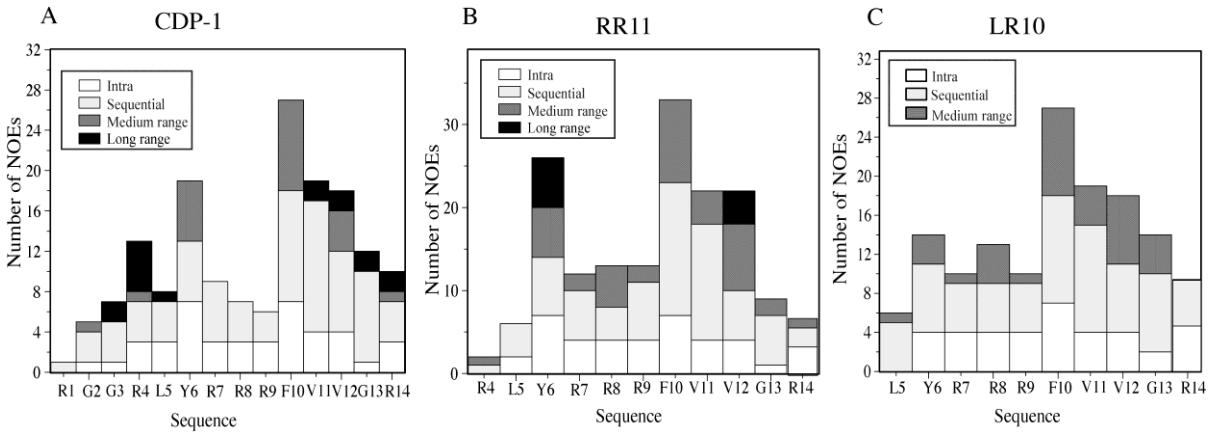
A
CDP-1
Intra
Sequential
Medium range
Long range
Number of NOEs
Sequence
R1 G2 G3 R4 L5 Y6 R7 R8 R9 F10 V11 V12 G13 R14
B
RR11
Intra
Sequential
Medium range
Long range
Number of NOEs
Sequence
R4 L5 Y6 R7 R8 R9 F10 V11 V12 G13 R14
C
LR10
Intra
Sequential
Medium range
Number of NOEs
Sequence
L5 Y6 R7 R8 R9 F10 V11 V12 G13 R14

Figure 7

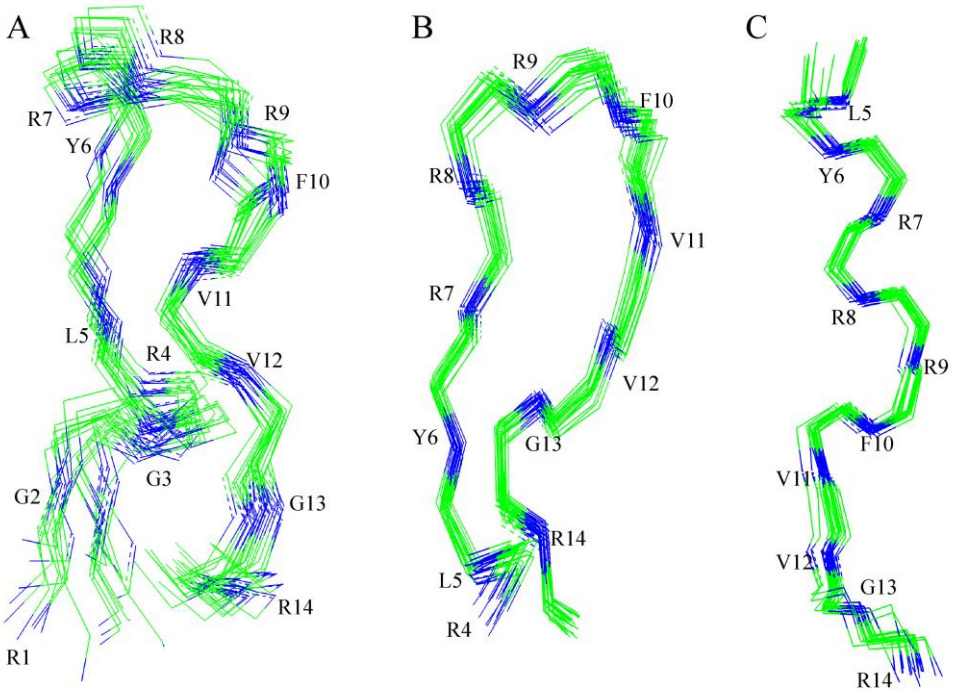
A
R8
R7
R9
Y6
F10
V11
L5
R4
V12
G3
G2
G13
R14
R1
B
R9
F10
R8
V11
R7
V12
Y6
G13
R14
L5
R4
C
L5
Y6
R7
R8
R9
F10
V11
V12
G13
R14

Figure 8

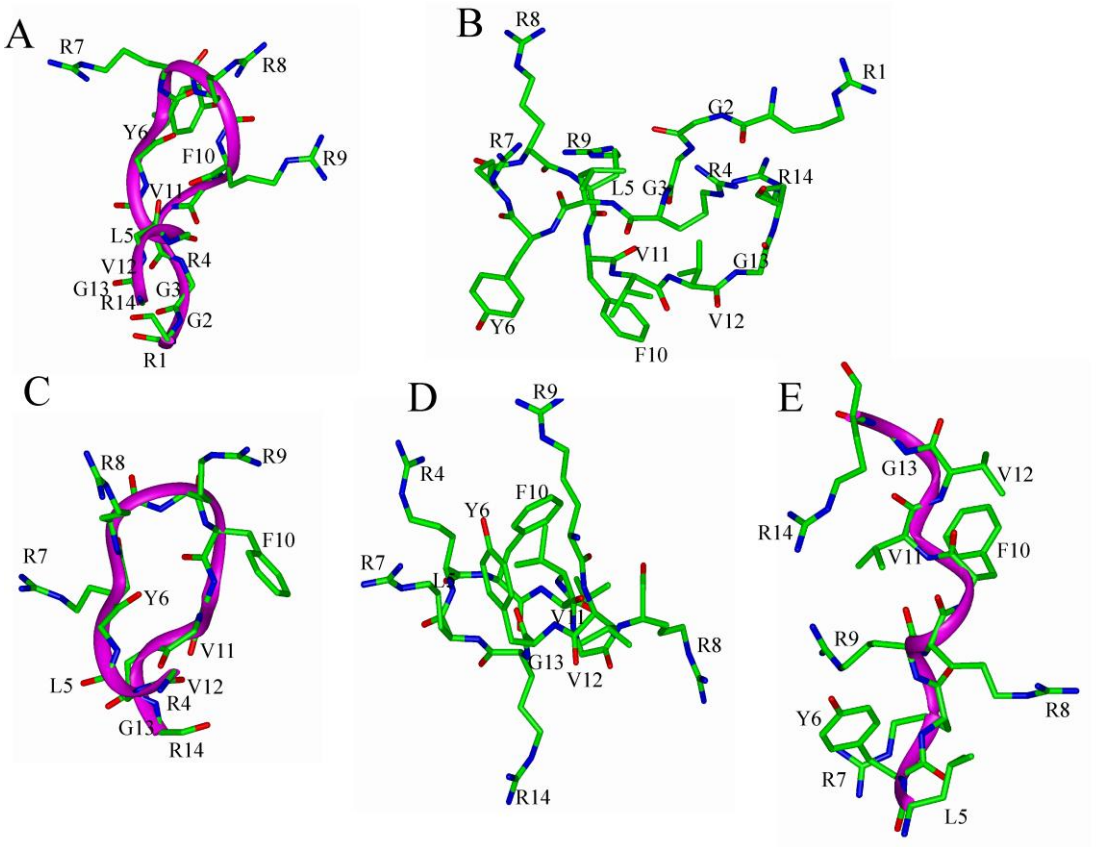
A
R7
R8
Y6
F10
R9
V11
L5
V12
R4
G13
G3
R14
G2
R1
B
R8
R1
G2
R7
R9
R4
R14
L5
G3
V11
G13
Y6
V12
F10
C
R8
R9
F10
R7
Y6
V11
L5
V12
R4
G13
R14
D
R9
R4
F10
Y6
R7
V11
R8
G13
V12
R14
E
G13
V12
R14
V11
F10
R9
R8
Y6
R7
L5

Figure 9